CONF-900563--7

DE90 011174

CONF-900563--7

MAY 2 9 1990

DEVELOPMENTS IN RADIATION HODOSCOPE TECHNOLOGY FOR ARMS CONTROL TREATY VERIFICATION *

Charles. E. DICKERMAN, Edgar A. RHODES, George S. STANFORD, and Alexander DEVOLPI

Reactor Analysis & Safety Division, Argonne National Laboratory, Argonne, IL, 60439, USA

New hodoscope radiation detection technology developments offer a wide range of unique capabilities for arms control treaty verification (ACTV). Originally developed for civilian nuclear power research by Argonne National Laboratory, this concept uses a radiation detector array to detect objects inside opaque containments. To avoid unnecessary intrusiveness in treaty verification, spatial resolution must be limited and confirmed. Material density data and identification by radiation means may be either required or prohibited. ACTV instruments also should be inherently resistant to false indications--either accidental, or from attempts at deception. Hodoscope technology can meet these needs.

ACTV hodoscopes do not require the heavy collimators of reactor hodoscopes, and relatively weak sources are sufficient. Gamma-ray transmission hodoscopes can be used to inspect canisters, railcars, etc. or to monitor objects such as rocket motors. This technique is deception-resistant: absorbers hidden to mask objects will be detected; and sources hidden to mask absorption will be subtracted out as background. Nuclear warheads are detectable by strong gamma-ray absorption. In some cases, intrinsic gamma-ray radiation from warheads also could be used in a passive mode. Neutron hodoscopes can utilize neutron transmission, intrinsic neutron emission, or neutron reactions (either prompt or delayed) stimulated by a neutron source. Warheads can be counted by tomography, or by simple analysis of count rate curve patterns, depending on application. Hodoscope technology is a powerful tool for potential treaty verification uses. Optimization for specific cases can be considered.

* Work supported by the U.S. Department of Energy, Technology Support programs under Contract W-31-109-Eng-38. The work reported herein is part of a research and development program for arms control and treaty verification and does not imply current or future policy positions or technical preferences of any agency of the U.S. government.

MASTER

DISTRIBUTION OF THIS DOCUMENT IS UNLIMITED

1. Introduction

Many potential arms control treaty verification (ACTV) applications may be described in terms of a generic requirement to identify or distinguish between objects located within opaque enclosures, under conditions in which direct observation may not be convenient (or even permitted under the terms of the treaty). Special restrictions may be placed on the identification technique in order to limit the extent of information provided by the verification inspection in such items as: spatial resolution, density, or composition. In some cases, the treaty may require data on specific elements or isotopes in order to provide a clear identification of a specific object as a treaty limited item (TLI). Because of our extensive experience with hodoscope technology for radiation imaging, we have conducted a number of experiments of a generic nature in order to demonstrate the capability of hodoscope systems for potential ACTV applications.

For many years, a hodoscope system has been used in civilian nuclear power development research at the U.S. Department of Energy TREAT reactor built and operated by Argonne National Laboratory.[1] A hodoscope system was later installed in the CABRI reactor in France for similar work.[2] These systems use arrays of radiation detectors arranged to "image" movements of test specimens located in the test reactor core, inside opaque containers. The term, hodoscope, was adopted to describe these systems by analogy with hodoscopes used in cosmic ray research to study the directional and spatial characteristics of cosmic ray air showers. For ACTV applications, a hodoscope array may view radiation emitted by a radioactive specimen, radiation induced and emitted by the specimen (e.g., as a result of neutron bombardment), or radiation transmitted from a source (or accelerator) behind the specimen and thus attenuated by the spatial distribution of absorber in the specimen.

In some respects, ACTV requirements are significantly less demanding than those of reactor development. First, there is no intense reactor background radiation that requires the use of extensive, heavy shielding and radiation collimators. Next, we would expect the TLI to be static or quasi-static; so there is no requirement for special data acquisition systems recording data at rates as short as a millisecond per frame. When this consideration is combined with low background plus coarse spatial resolution, we are able to utilize relatively low count rates from low level sources while achieving readily acceptable counting times. Finally, we would expect that there would be

limitations on the space resolution of the TLI measurement, which would simplify considerably the design and operation of the instrument, and would eliminate apparatus for scanning across the test specimen region. In either case, the use of an array with individual detectors counting simultaneously rather than in sequence results in a considerable savings in overall measurement time. In this paper, we will restrict the discussion to fixed array hodoscope systems, whose space resolution is set by mechanical design, and which may be checked readily. It should be noted that spatial resolution much higher than that described below could be designed into the system, if it were needed.

Three generic situations were identified for the demonstration measurements: discrimination between a nuclear warhead and a conventional high explosive warhead; low-resolution diameter measurements of rocket motors located inside a missile cannister which, in turn is located inside a railcar; and counting nuclear warheads. The nuclear warheads were simulated by non-fissile mockups based on the "model nuclear warhead" characteristics recommended by Sagdeev et.al. for generic ACTV studies.[3] We make no comment on the possible degrees of accuracy of that reference; we use it only to provide consistency with published unclassified generic ACTV literature. Two modes of operation were selected for our measurements: gamma-ray transmission and neutron reaction. Supporting analyses included neutron reaction calculations and tomographic reconstruction calculations. Attention was given to generic resistance to attempts at deception.

2. Gamma-ray Transmission Measurements

The gamma-ray transmission hodoscope consisted of a Co-60 source, along with a 25-channel linear array of 2-cm diameter photomultiplier tubes optically coupled directly to 2-cm-long NaI scintillator crystals. Crystal centerlines were spaced at 4-cm intervals. With the test object half-way between source and detectors, this spacing corresponds to nominal 2 cm at the test object. The counting discriminator was set to include both the 1.17 and 1.33 MeV Co-60 peaks. Data were taken in the following sequence: First, background count rates with no source or object were recorded. Then reference count rates were taken with the source but no object. Last, the object count rates were taken with source and object. Ratios of object rate minus background, N, to reference count rate minus background, No, were calculated for each detector. It is convenient for display and discussion

to use the equivalent absorption per detector, with is equal to the negative of the natural logarithm of these count rate ratios.

Scoping measurements were made with a lucite and lead test object to confirm that the interface between the lead and the relatively high-scattering lucite could be detected readily with uncollimated gamma-ray detectors.

The first actual demonstration measurement was performed with a non-fissile mockup of the Sagdeev model. The model heavy metal gamma-ray absorption was simulated by a lead spherical shell with outer and inner diameters of 20 cm and 10 cm, respectively. Measurements were taken with a 50-cm diameter steel can filled with sand to simulate the gamma-ray absorption and scattering of materials such as missile fuel, high-explosive [3], etc. Runs with and without the lead object showed that the heavy metal was readily detected despite being embedded in a large scattering volume. Fig. 1 shows relative absorption data both with and without the lead. Although there is an indication of decreased absorption in the sphere center, design detail is not apparent. These results illustrate the use of this technique to distinguish between a chemical high-explosive and a nuclear warhead.

The next demonstration consisted of a full-scale mockup of rocket motor stages inside a canister in a railcar. In the absence of a specific set of application requirements, the stage diameters used open-literature data [4] on the Soviet SS-20 intermediate range missile, which is prohibited under the INF Treaty. The generic missile stages were made of three half-cylinders located adjacent to each other on a common centerline. All were contained within a fourth half-cylinder ("canister"). Construction material for all four was 6.35 mm steel plate. The three "missile stage" cylinders were filled with sand to simulate gamma-ray absorption and scattering by solid rocket motor fuel. Two 4.76 mm steel plates, one at the source and one at the detector array simulated the "railcar" walls. Nominal outer diameters of the canister and three stages are 1025 mm, 903 mm, 778 mm, and 743 mm, respectively. Data were taken using 10 millicurie and 20 millicurie Co-60 sources, adequate to permit convenient counting times of about 1-3 minutes. Source to array distance was 4 meters. Data were taken at fourteen slices along the test object, with particular attention to the interface regions between two adjacent "stages". No artifacts were found in these interface regions. Fig. 2 shows absorption data from four slices, superimposed on a side view of the test object.

Data from slices 6 and 9 are typical and are displayed on a larger scale in Figs. 3 and 4. The stage diameters are seen clearly with an uncertainty of about a half-channel (one cm.).

3. Neutron-reaction Measurements

Non-fissile generic warhead objects based on the Sagdeev model were prepared using one Cf-252 source inside each object. Each source emits approximately 500,000 neutrons per s, resulting in counting times of the order of 1-3 minutes. A spherical shell 5-10 cm thick outside the lead contained granulated, high-purity graphite to simulate the neutron absorption and scattering (moderating) characteristics of chemical high explosives.[5] Neutrons emitted from the objects simulate intrinsic neutrons emitted from the warheads, prompt neutrons from fissions stimulated by an external source, or delayed neutrons from stimulated fissions. Three such objects were used in simple configurations: (1) one object, (2) two objects side by side, (3) two objects in line with the detector, (4) three in an equilateral triangle scanned along a base, and (5) equilateral triangle scanned parallel to an altitude. These data may then be combined to construct the results of measurements on more complicated configurations, as desired.

Measurements were taken with a 12.5 cm diameter by 12.5 cm long NE213 liquid scintillator. The detector was collimated with an 83.8-cm-long borated polyethylene cylinder with 10-cm bore, to which was attached a 10-cm-long steel front section. Fig. 5 is the block diagram of the system, showing the pulse shape discriminator (PSD) system for rejection of gamma background.

Comparison of plots of count rate *vs* position from configurations (1) and (3) showed that one object effectively eclipses another located behind it. Fig. 6 presents combined plots of count rate *vs* transverse position for the two triangle configurations. Representative error bars are shown. Configuration (5) illustrates that one object eclipses another. The low peak associated with the single object results from the $1/R^2$ dependence of the signal strength, where R is the source to detector distance. Note that the count rate curves show clearly-distinguishable indications of the individual objects; thus, it appears that the shapes of data plots from properly spaced hodoscope detectors are adequate for some warhead counting applications without tomographic reconstruction.

4. Neutron-reaction Calculations

Standard reactor physics computer techniques were used to confirm the choice of high purity granulated carbon (i.e., to assure that the spectrum of the neutron flux emitted by the non-fissile mockup objects simulated that from fissile-material-containing Sagdeev model objects).[6, 7, 8, 9] Then, calculations were made to determine detectability of fissile Sagdeev model objects by a generic, transportable, neutron-reaction hodoscope with shielded and collimated neutron sources and detectors. Calculations considered source strength and spectra for candidate sources, computations of neutron flux magnitude and spectra for prompt and delayed neutrons emitted by the Sagdeev objects, detector efficiency and spectral response, collimator and shielding performance, and total background.[10-19] Measurement times then were calculated for statistically significant detection in several cases. Table 1 summarizes the results for two stimulating sources: an Am-Li radioactive source (note that, because of typical source self-absorption for strengths in excess of 1 million neutrons/s and to provide more unifirm stimulation, the table uses 10 sources located around the objects, rather than a single large source); and a D-T accelerator source. Measurements of neutrons from fissions stimulated by the radioactive source are made with neutron energy pulse-height discrimination to count only fission neutrons with energy above 1.5 MeV in order to discriminate against source neutrons scattered back into the detector. Measurements using the accelerator neutrons for stimulation rely upon detection of delayed neutrons from the stimulated fission; an accelerator cycle of about 3 s irradiation time plus 3 s counting time, (with short delay times between irradiation and counting) was found to be near optimum. Measurement times for the four cases in Table 1 are quite acceptable.

5. Tomographic reconstruction analyses

Scoping tomography analyses were for a range of gamma-ray absorption and neutron-reaction cases, using standard reconstruction algorithms, with emphasis on the use of very coarse resolution data in order to count objects without obtaining accurate representations of size and shape. [20] Fig. 7 shows the results of tomographic reconstruction of three of the simulated neutron-reaction generic objects, obtained using experimental data from three views. Corrections were made for neutron absorption in the objects using standard cross section data [21], and the CONGR algorithm [20]. Fig. 7 shows three

objects in the correct locations, but size and shape are not imaged with any degree of precision.

6. Resistance to attempts at deception

Although each potential application would need to be analyzed in detail for resistance to attempts at deception, certain favorable generic characteristics of these hodoscope systems can be identified:

Gamma-ray transmission hodoscopes will detect absorbers hidden to mask objects; and sources hidden to compensate for absorption will be subtracted out as background by the procedure described in section 2. Care must be taken to guard against attempts to make a TLI appear to be a larger, permitted, item.

Neutron-reaction hodoscopes will show anamolies if neutron absorbers are hidden to mask a warhead. An example of one such situation is shown in Fig. 8, in which a fourth warhead with masking absorber is hidden in the middle of a three-warhead array. The masked warhead will eclipse a normal one, causing a given normal warhead to appear and disappear, depending on viewing position.

7. Discussion

The demonstration measurements described herein show that the test reactor hodoscope concept can be successfully adapted to provide a capability for a wide range of ACTV applications. It is now appropriate to go beyond generic demonstrations to design-related measurements for specific TLIs and applications.

8. Acknowledgements

It is a pleasure to acknowledge the contributions of our co-workers, including T. H. Braid, R. C. Doerner, M. A. Kraimer, P. Melko, J. P. Regis, D. J. Travis, and J. P. Tylka. We also wish to thank A. Travelli, our ANL project manager, and L. Casey, our DOE program manager, for their support and guidance.

References

[1] A. DeVolpi, C. L. Fink, G. E. Marsh, E. A. Rhodes and G. S. Stanford, Nucl. Tech. 56 (1982) 141.
[2] K. Bohnel and H. Blum, Proc. 1979 Int. Mtg. Fast Reactor Safety Tech, Seattle, WA Vol V (1979) 2261.

[3] R. Z. Sagdeev, O. F. Prilutskii and V. A. Frolov, "Problems of Monitoring sea-based Cruise Missiles with Nuclear Warheads", Fed. Amer. Scientists seminar, Key West, FL (1988).
[4] SS-20 "Saber", Janes' Strategic Weapon Systems, USSR: Offensive Weapons (1989).
[5] B. M. Dobratz, ed., "Properties of Chemical Explosives and Explosive Simulants", Lawrence Livermore Laboratory report UCRL-51319 Rev. 1 (1974).
[6] B. A. Zolotar, W. R. Cobb, W. J. Eich, and D. E. Tive, "EPRI-CELL Code Description", Advanced Recycle Methodology Program System Documentation, Part II, Chapter 5, Electric Power Research Institute (1977).
[7] R. E. MacFarlane, C. W. Muir, and R. M. Boicourt, "The NJOY Nuclear Data Processing System, Vol I: User's Manual", Las Alamos National Laboratory report LA-9303-M, Vol I (ENDF-324) (1982).
[8] R. E. Alcouffe, F. W. Brinkley, D. R. Marr and R. D. O'Dell, "User's Guide for TWODANT: A Code Package for Two-dimensional, diffusion-accelerated Neutral-particle Transport", Los Alamos National Laboratory report LA-10049-M (1988).
[9] R. N. Blomquist, R. M. Lell, and E. M. Gelbard, "VIM-A Continuous Energy Monte Carlo Code at ANL", Oak Ridge National Laboratory report ORNL/RSIC-44, (1980), 31.
[10] H. Ing, W. G. Cross, and B. J. Tymons, "The Spectrum of Neutrons from a Pu-238/Li Source", Health Physics 40 (1981) 345.
[11] M. E. Anderson, "Neutron Energy Spectra of PU-239/Be, Pu238/F, and Pu238/0-18(alpha, n) Sources", Mound Laboratory ACE R&D report MLM-1422 (1967).
[12] K. Geiger and L. Van der Zwan, "The Neutron Spectra and the Resulting Fluence-kerma Conversions for Am-241/Li(alpha, n) and Po-210/Li(alpha, n) Sources", Health Physics 21 (1971) 120.
[13] V. M. Gorbachev, Y. S. Zamyatnin, and A. A. Lbov, Nuclear Reactions in Heavy Elements (Pergamon, Oxford, 1980).
[14] D. Safier, D. Ilberg, S. Shalev, and S. Yiftah, "Evaluated Delayed Neutron Spectra and Their Importance to Reactor Calculations", Nucl. Sci. & Engr. 62 (1977) 660.
[15] G. F. Knoll, Radiation Detection and Measurement, 2nd Ed. (John Wiley & Sons, New York, 1989).
[16] M. Drosg, "Accurate Measurements of the Counting Efficiency of a NE-213 Neutron Detector between 2 and 26 MeV", Nucl. Instr. & Meth. 105 (1972) 573.
[17] J. L. Fowler, J. A. Cookson, M. Hussain, R. B. Schwartz, M. T. Swinhoe, C. Wise, and C. A. Uttley, "Efficiency Calibration of Scintillation Detectors in the Neutron Energy Range 1.5-25 MeV by the Associated Particle Method", Nucl. Instr. & Meth. 175 (1980) 449.

[18] M. Yamashita, L. D. Stephens, and H. W. Patterson, "Cosmic-ray-produced Neutrons at Ground Level: Neutron Production Rate and Flux Distribution", J. Geophys. Res. 71 (1966) 3817.
[20] J. Kastner, B. G. Oltman, and L. D. Marinelli, "Progress Report on Flux and Spectrum Measurements of the Cosmic-ray Neutron Background", in The National Radiation Environment (University of Chicago, Chicago, 1964).
[21] R. H. Huesman, G. T. Gullberg, W. L. Greenberg, and T. F. Budinger, "Donner Algorithms for Reconstruction Tomography", Lawrence Berkeley Laboratory Pub. 214 (1977).

Table 1. Results of 2-D TWODANT/RESPONSE Computations

Sources:	^{241}Am-Li (depleted ^{17}O and ^{18}O)	D-T accelerator
Detectors:	12.7 cm x 12.7 cm NE213 (psd)	same or 12.7 cm diam. thermal
Measurement Cycle:	continuous	6 s
Tomographic Counting of Warheads in an Array, Transportable Hodoscope System		
Detection geometry:	Avg. source-object = 1 m = avg. source-detector, object-detector = 3 m (right angles to source)	
Source Strength:	10^7 n/s (10 sources)	1.44 x 10^9 n/s
Shielding:	20 cm CH_2 - LiH	10 cm CH_2 - LiH
Measurement Time:	2.2 min (29 min for 12 views)	2.0 min (27 min for 12 views)
Signal/Background:	2.77	1.21
Detection of Warhead, Portable Hodoscope		
Detection geometry:	Source-object = 37.7 cm = object-detector, source-detector = 53.3 cm	
Source Strength:	10^6 n/s	
Shielding:	10 cm CH_2 - LiH	
Measurement Time:	26 sec	
Signal/Background:	3.13	

Fig. captions

1. Results of demonstration measurement on discrimination between generic (lead) nuclear warhead model and sand mockup of chemical high-explosive/missile fuel.

2. Typical results of demonstration measurement on discrimination between missile stage diameters.

3. Results of slice 6 data from missile stage diameter measurements.

4. Results of slice 9 data from missile stage diameter measurements.

5. Block diagram of electronic counting system for neutron-reaction system measurements.

6. Schematic layout showing neutron hodoscope results for three generic (Cf-252, lead and graphite) mockups of nuclear warheads.

7. Attenuation-corrected emission tomographic reconstruction of neutron hodoscope experimental data from three generic mockups of nuclear warheads.

8. Schematic layout showing detection of attempt to hide a nuclear warhead within an array. Three objects are arranged with a fourth (central) object which is masked by neutron-absorber. Because one object eclipses another when they are in line with the detector, the masked central object will eclipse one of the normal objects when they are at least partially in-line; and this results in a normal object appearing and disappearing when different views are compared. For example, object A is visible in view 3, but disappears in view 1.

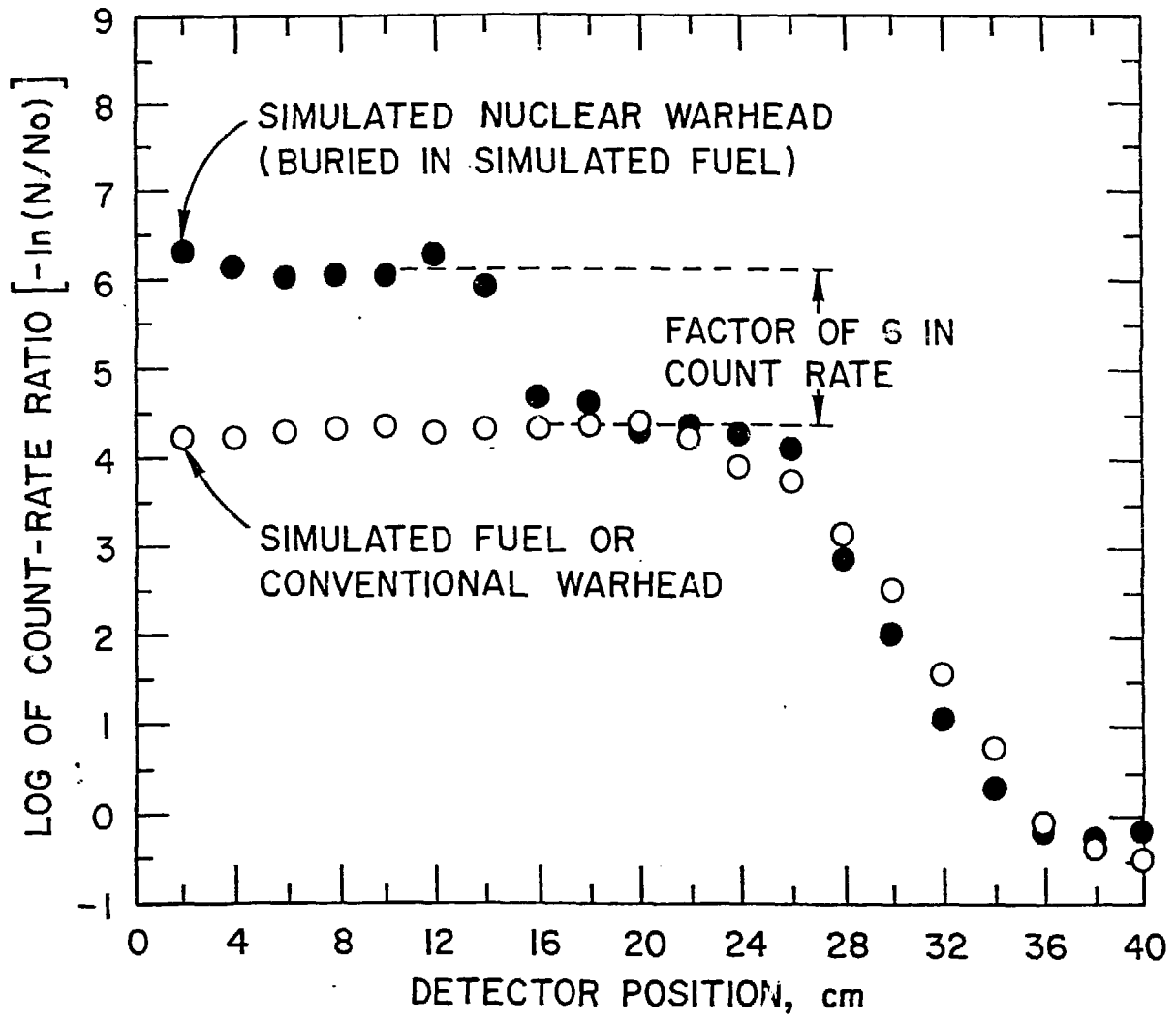

Fig. 1. Results of demonstration measurement on discrimination between generic (lead) nuclear warhead model and sand mockup of chemical high-explosive/missile fuel.

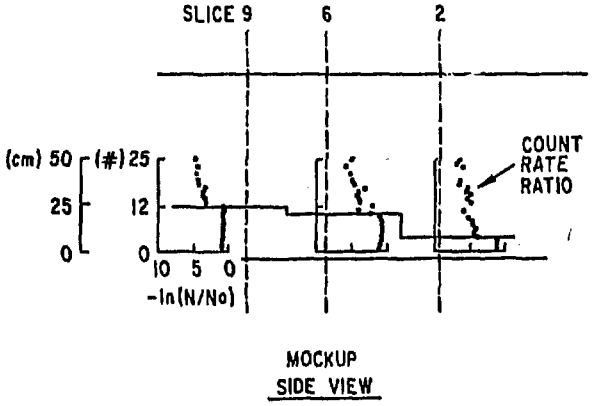

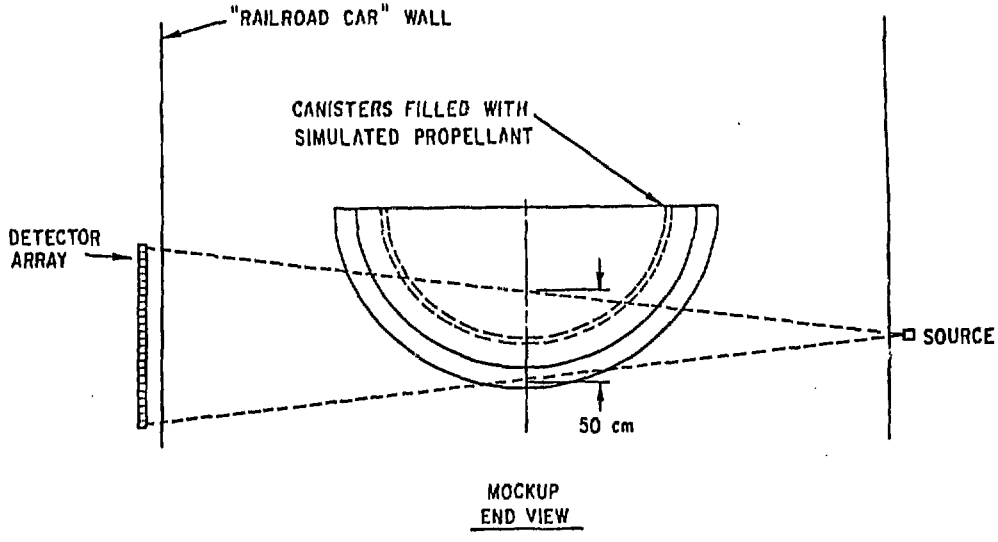

Fig. 2. Typical results of demonstration measurement on discrimination between missile stage diameters

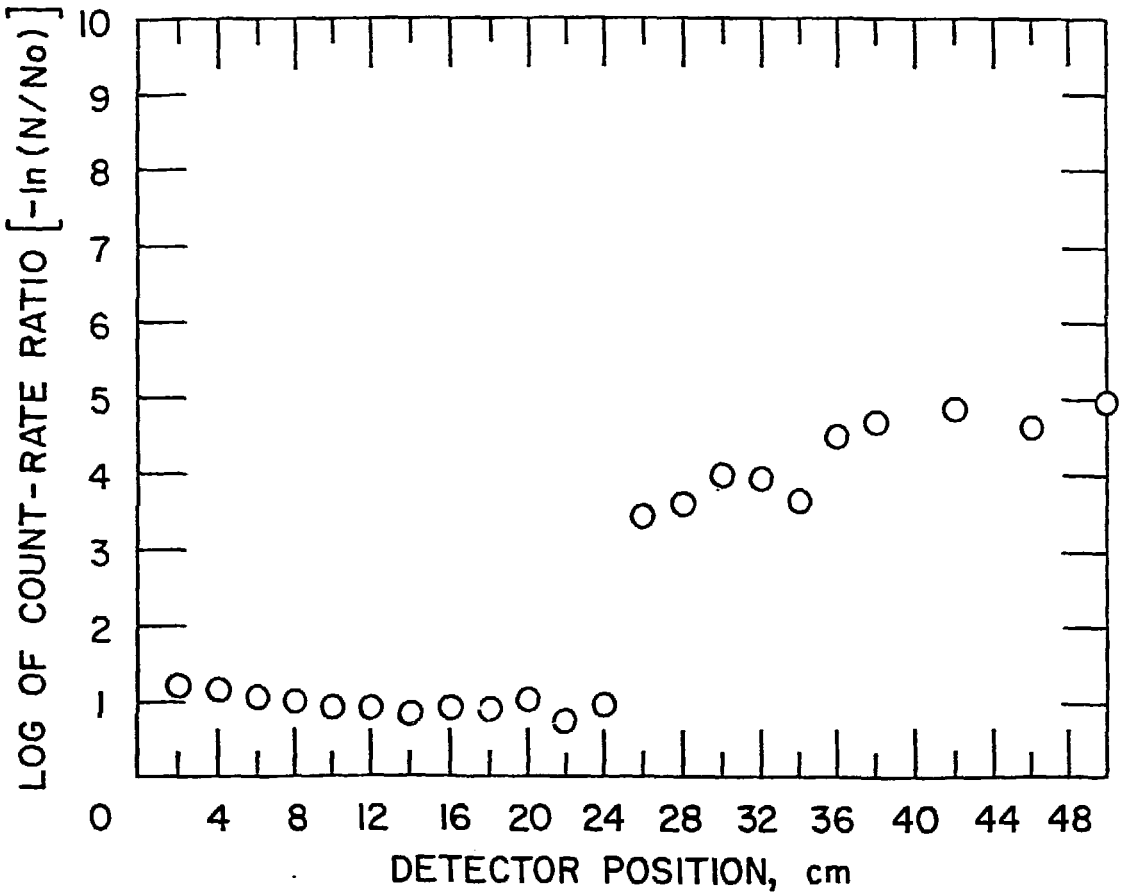

Fig. 3. Results of slice 6 data from missile stage diameter measurements.

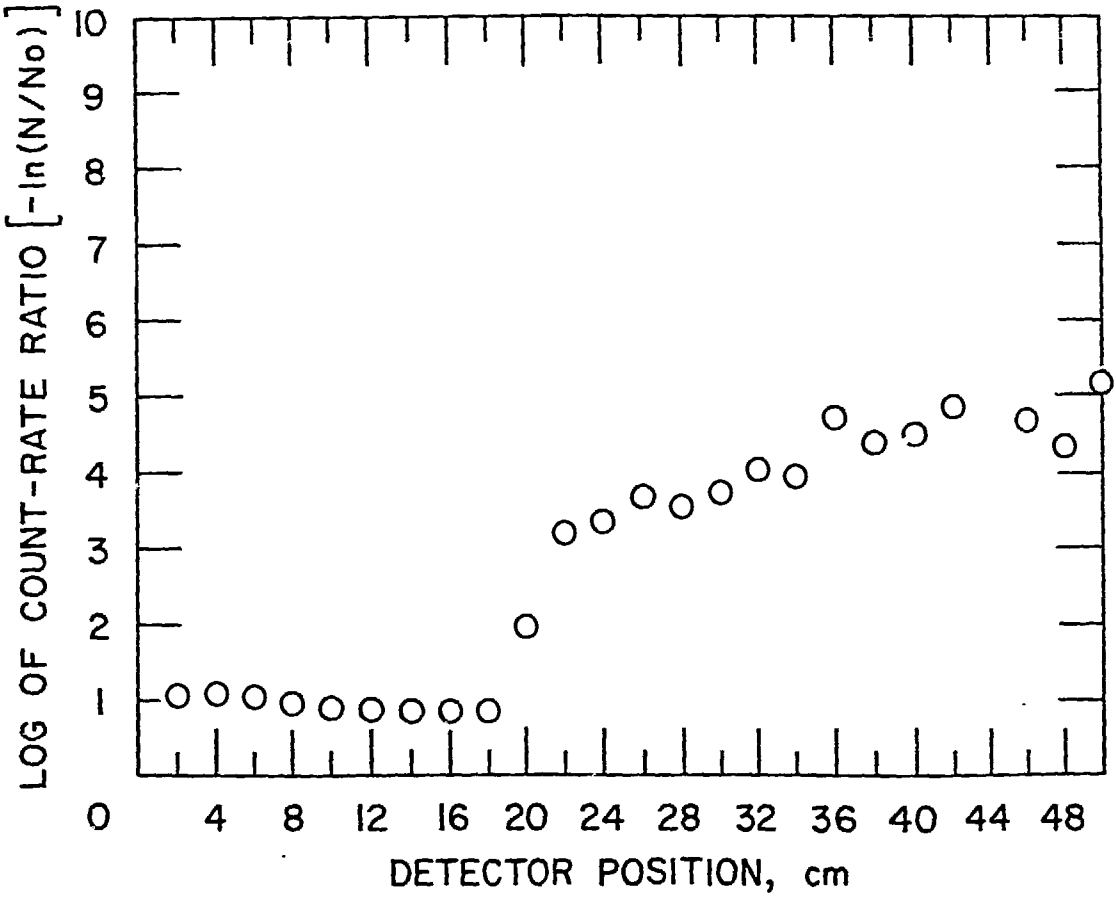

Fig. 4. Results of slice 9 data from missile stage diameter measurements.

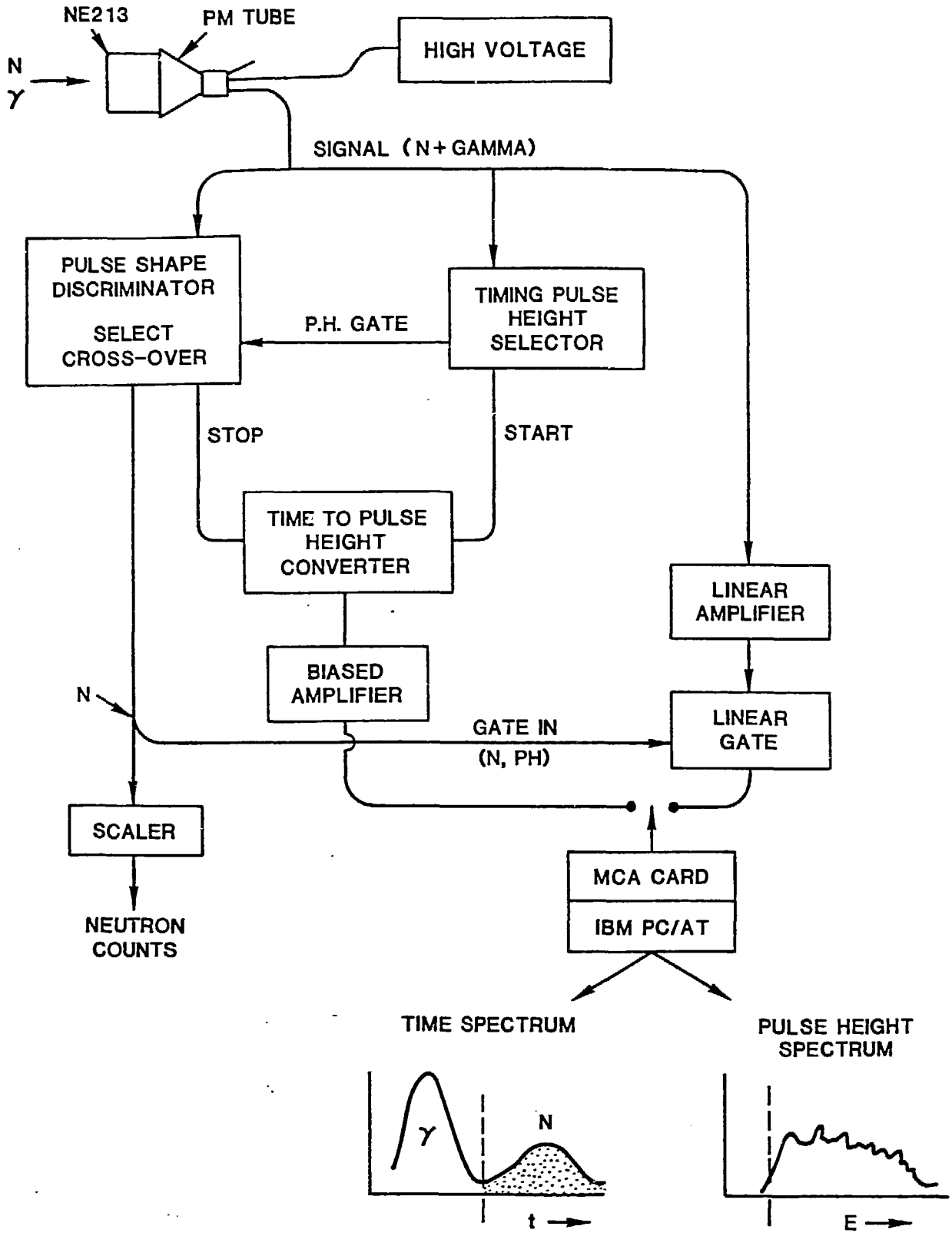

Fig. 5. Block diagram of electronic counting system for neutron-reaction system measurements.

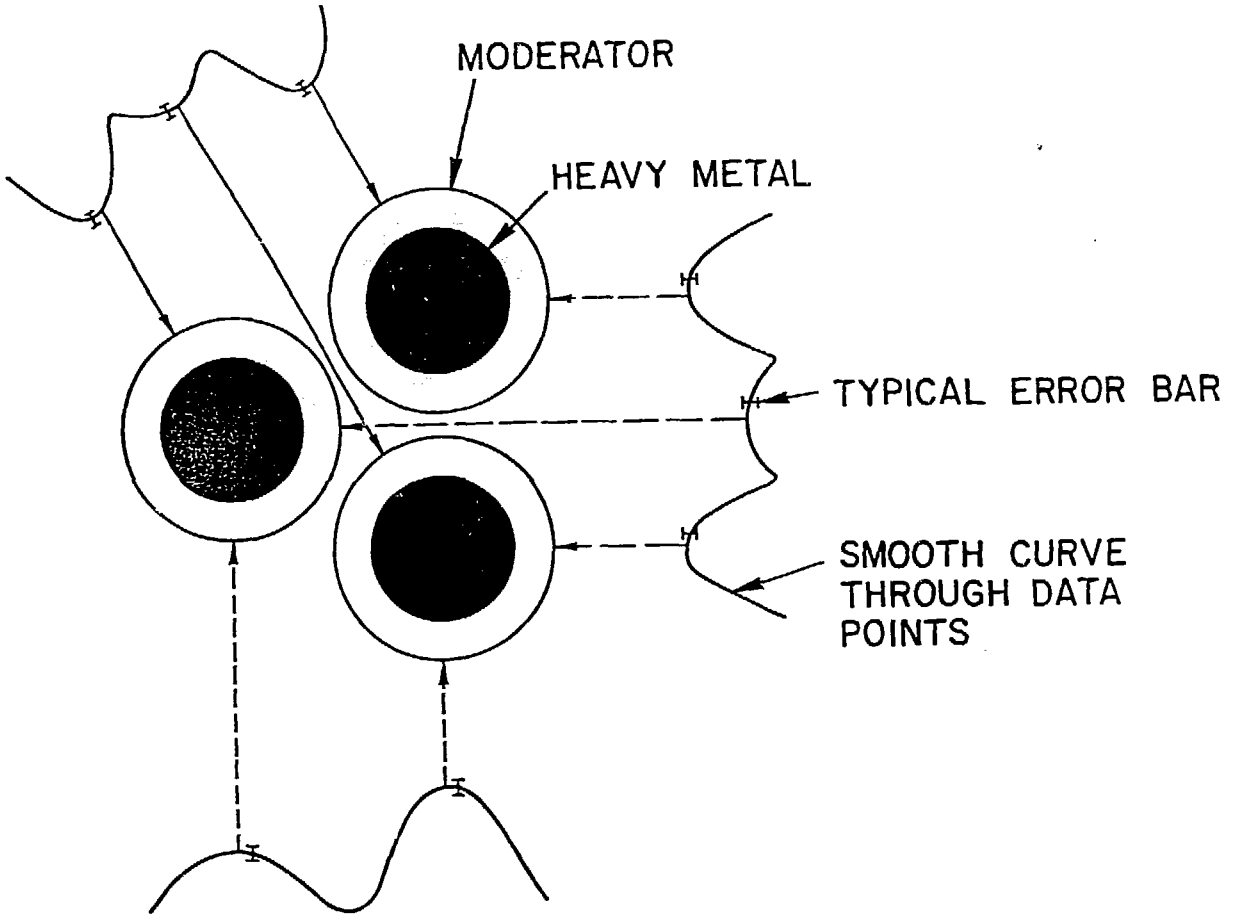

Fig. 6. Schematic layout showing neutron hodoscope results for three generic (Cf-252, lead and graphite) mockups of nuclear warheads.

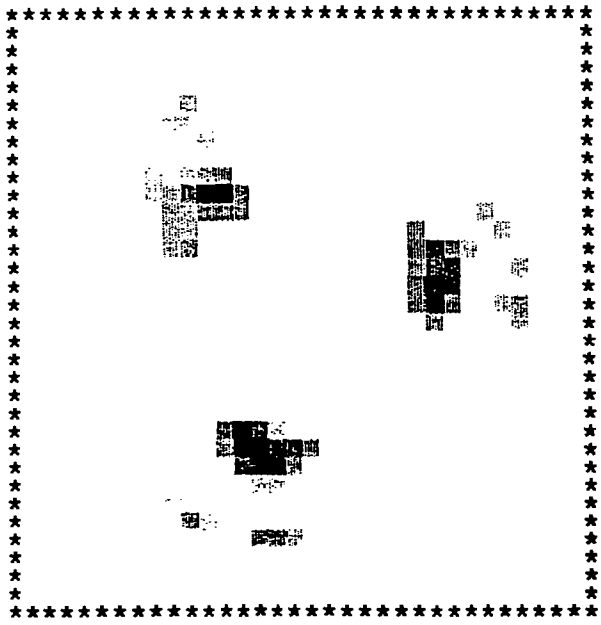

Fig. 7. Attenuation-corrected emission tomographic reconstruction of neutron hodoscope experimental data from three generic mockups of nuclear warheads.

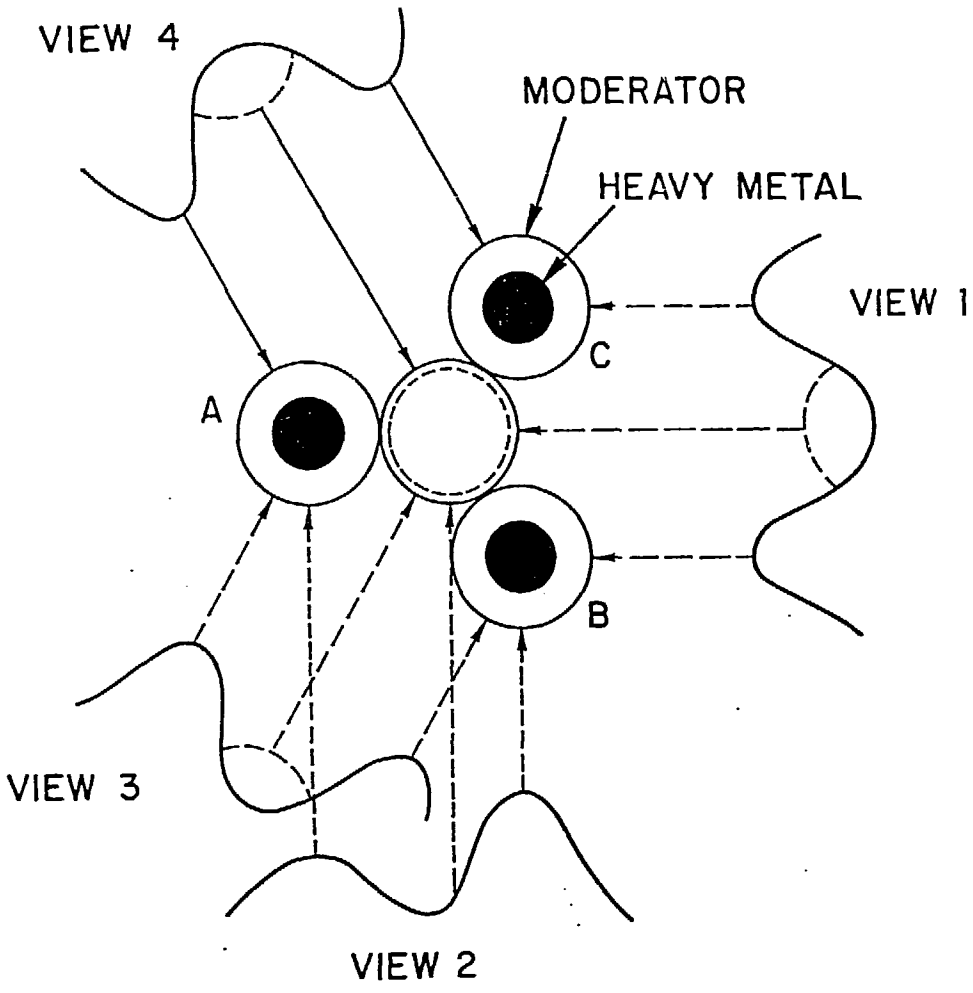

Fig. 8. Schematic layout showing detection of attempt to hide a nuclear warhead within an array. Three objects are arranged with a fourth (central) object which is masked by neutron-absorber. Because one object eclipses another when they are in line with the detector, the masked central object will eclipse one of the normal objects when they are at least partially in-line; and this results in a normal object appearing and disappearing when different views are compared. For example, object A is visible in view 3, but disappears in view 1.